Available online at www.sciencedirect.com
ScienceDirect
International Journal of Heat and Mass Transfer 50 (2007) 4688–4697
International Journal of HEAT and MASS TRANSFER
www.elsevier.com/locate/ijhmt

Natural convection in a rectangular cavity with partially active side walls

N. Nithyadevi, P. Kandaswamy *, J. Lee

School of Mechanical Engineering, Yonsei University, Seoul 120-749, Republic of Korea
UGC-DRS Centre for Fluid Dynamics, Department of Mathematics, Bharathiar University, Coimbatore 641 046, India

Received 16 October 2006; received in revised form 2 March 2007
Available online 18 June 2007

Abstract

A numerical study is performed to investigate the effect of aspect ratio on the natural convection of a fluid contained in a rectangular cavity with partially thermally active side walls. The active part of the left side wall is at a higher temperature than that of the right side wall. The top and bottom of the cavity and inactive part of the side walls are thermally insulated. Nine different relative positions of the active zones are considered. The equations are discretized by the control volume method with power law scheme and are solved numerically by iterative method together with a successive over relaxation (SOR) technique. The results are obtained for Grashof numbers between 10^3 and 10^5 and the effects of the aspect ratio on the flow and temperature fields and the rate of heat transfer from the walls of the enclosure are presented. The heat transfer rate is high for the bottom–top thermally active location while the heat transfer rate is poor in the top–bottom thermally active location. The heat transfer rate is found to increase with an increase in the aspect ratio.

Keywords: Natural convection; Partially active walls; Aspect ratios; Rectangular cavity

1. Introduction

A natural convection flow that has engineering and geophysical applications is that arising in a rectangular cavity with differentially heated side walls. In the fields like solar energy collection and cooling of electronic components, the active walls may be subject to abrupt temperature non-uniformities due to shading or other effects. With a view to understand the above problem, we shall first look into the studies related to the above problem. The effect of the aspect ratio on the two-dimensional steady natural convection in a porous rectangular cavity is numerically analyzed by Prasad and Kulacki [1]. Multicellular flow has been found for $A \leqslant 1$ and the flow structure comprises a primary recirculating cell with smaller secondary cells inside. The Nusselt number is always increased when the aspect ratio is increased and this increase is more rapid in shallow cavities than in tall cavities.

Paolucci and Chenoweth [2] studied the natural convection in shallow enclosures with differentially heated end walls. They find that the classical parallel flow solution, accurate in the core of the cavity in the Boussinesq limit, does not exist when variable properties are introduced. Ho and Chang [3] numerically and experimentally studied the effect of aspect ratio of natural convection heat transfer in a vertical rectangular enclosure with two-dimensional discrete heating. Numerical simulation is conducted for aspect ratio varying from 1 to 10 with given relative heater size and location. From the numerical simulation, they find that the effect of enclosure aspect ratio on the average Nusselt number of the discrete heaters tends to decrease with the increase of the modified Rayleigh number. The predicted temperature and flow fields were found to be in good agreement with the experiments.

* Corresponding author. Address: UGC-DRS Centre for Fluid Dynamics, Department of Mathematics, Bharathiar University, Coimbatore 641 046, India. Tel.: +91 422 2426764; fax: +91 422 2422387.
E-mail address: pgkswamy@yahoo.co.in (P. Kandaswamy).

0017-9310/$ - see front matter © 2007 Elsevier Ltd. All rights reserved.
doi:10.1016/j.ijheatmasstransfer.2007.03.050

Nomenclature

g	acceleration due to gravity
Gr	Grashof number
H	height of the cavity
L	length of the cavity
Nu	local Nusselt number
$\overline{Nu}$	average Nusselt number
p	pressure
Pr	Prandtl number
t	time
T	dimensionless temperature
u, v	velocity components
U, V	dimensionless velocity components
x, y	coordinates
X, Y	dimensionless coordinates

Greek symbols

α	angle of inclination
β	coefficient of thermal expansion
κ	thermal diffusivity
ν	kinematic viscosity
ω	vorticity
ψ	stream function
Ψ	dimensionless stream function
ρ	density
τ	dimensionless time
θ	temperature
ζ	dimensionless vorticity

Subscripts

c	cold wall
h	hot wall

A numerical study of natural convection of air in rectangular cavities was conducted by Frederick [4]. He concludes that the overall Nusselt number decreases rapidly with increasing aspect ratio. The circulation rate increases always with the Rayleigh number and with aspect ratio. Tong [5] studied the effect of the aspect ratio on natural convection in water near its density maximum. He concludes that aspect ratio has a strong impact on the flow patterns and temperature distributions in rectangular enclosures. Wakitani [6] numerically presented oscillatory natural convection at low Prandtl number in rectangular enclosures. His numerical results agreed with available experimental results.

Effect of the surface waviness and aspect ratio on heat transfer inside a wavy enclosure is studied numerically by Das et al. [7]. They show that the heat transfer is changed considerably when the surface waviness changes and also depends on the aspect ratio of the domain. Effect of the aspect ratio of thermal–fluid transport phenomena in cavities under reduced gravity is studied numerically by Torii [8]. Valencia and Frederick [9] numerically analyzed the natural convection of air in a square cavity with partly thermally active side walls for five different heating locations. They find that the heat transfer rate is enhanced when heating location is at the middle of the hot wall.

El-Refaee et al. [10] studied numerically natural convection in a partially cooled, differentially heated inclined cavities with different aspect ratios. Deng et al. [11] numerically studied steady state laminar natural convection in a rectangular enclosure with discrete heat sources on the wall. They conclude that the role of isothermal heat sources is generally much stronger than the flux of heat sources.

Nithyadevi et al. [12] studied natural convection in a square cavity with partially active side walls. Kandaswamy et al. [13] investigated maximum density effects of water in a square cavity with partial thermally active side walls. The present study describes the natural convection in a rectangular cavity with partially active side walls for nine different heating locations. That is, for the hot region located at the top, middle and bottom and the cold region moved from bottom to top, to locate the regions where the heat transfer rate is maximum and minimum. The results are displayed graphically in terms of the streamlines and isotherms, which show the effect of the aspect ratio with different heating locations of the side walls.

2. Mathematical formulation

A schematic diagram of the two-dimensional rectangular cavity of length L and height H filled with a fluid under investigation is shown in Fig. 1. The partially thermally active side walls of the cavity are maintained at two different but uniform temperatures, namely, θ_h and θ_c ($\theta_h > \theta_c$), respectively. The inactive parts of the side walls and horizontal walls $x = 0$ and $x = H$ are thermally insulated. Nine different cases will be studied here. That is, for the hot region located at the top, middle and bottom and the cold region moved from bottom to top. The length of the thermally active part is $H/2$. Representing the position through cartesian coordinate system and assuming all other fluid properties to be constant, the flow of an incompressible Boussinesq viscous fluid under the above specified geometrical and physical conditions is governed by the equations:

$$\frac{\partial u}{\partial x} + \frac{\partial v}{\partial y} = 0, \tag{1}$$

$$\frac{\partial u}{\partial t} + u\frac{\partial u}{\partial x} + v\frac{\partial u}{\partial y} = -\frac{1}{\rho_0}\frac{\partial p}{\partial x} + \nu\nabla^2 u - \frac{\rho}{\rho_0}g, \tag{2}$$

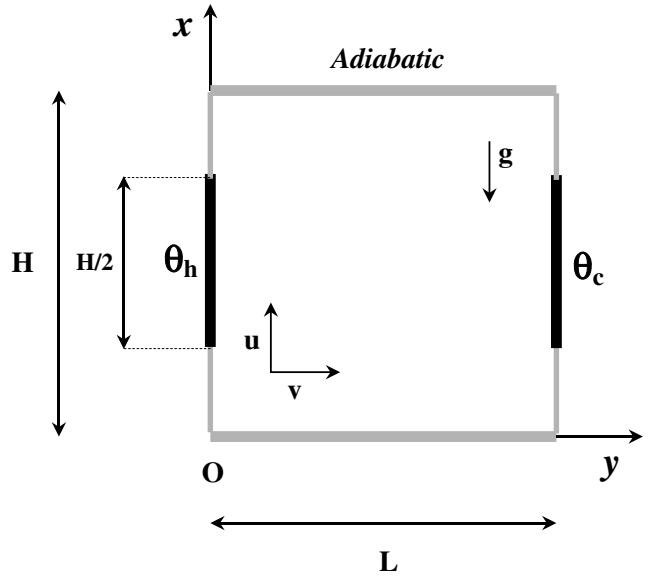

Fig. 1. Physical configuration.

$$\frac{\partial v}{\partial t}+u\frac{\partial v}{\partial x}+v\frac{\partial v}{\partial y}=-\frac{1}{\rho_0}\frac{\partial p}{\partial y}+\nu\nabla^2 v, \tag{3}$$

$$\frac{\partial \theta}{\partial t}+u\frac{\partial \theta}{\partial x}+v\frac{\partial \theta}{\partial y}=\alpha\nabla^2\theta, \tag{4}$$

$$\text{where}\quad \rho=\rho_0[1-\beta(\theta-\theta_c)]. \tag{5}$$

The appropriate initial and boundary conditions are

$$\begin{aligned}
&t=0: && u=v=0,\quad \theta=\theta_c,\ 0\leqslant x\leqslant H,\ 0\leqslant x\leqslant L,\\
&t>0: && u=v=0,\quad \frac{\partial\theta}{\partial x}=0,\ x=0 \text{ and } H,\\
& && \theta=\theta_h,\quad \text{on the hot part, } y=0,\\
& && \theta=\theta_c,\quad \text{on the cold part, } y=L,\\
& && \frac{\partial\theta}{\partial y}=0,\quad y=0 \text{ and } L.
\end{aligned}$$

Introducing the following non-dimensional variables $\tau=\frac{t}{L^2/\nu}$, $\Psi=\frac{\psi}{\nu}$, $\zeta=\frac{\omega}{\nu/HL}$, $U=\frac{u}{\nu H/L^2}$, $V=\frac{v}{\nu/L}$, $X=\frac{x}{H}$, $Y=\frac{y}{L}$, $T=\frac{\theta-\theta_c}{\theta_h-\theta_c}$, with $\theta_h>\theta_c$, we get the vorticity–stream function formulation of the above problems (1)–(5) as

$$\frac{\partial\zeta}{\partial\tau}-\frac{\partial\Psi}{\partial Y}\frac{\partial\zeta}{\partial X}+\frac{\partial\Psi}{\partial X}\frac{\partial\zeta}{\partial Y}=\frac{1}{Ar^2}\frac{\partial^2\zeta}{\partial X^2}+\frac{\partial^2\zeta}{\partial Y^2}+GrAr\frac{\partial T}{\partial Y}, \tag{6}$$

$$\frac{\partial T}{\partial\tau}-\frac{\partial\Psi}{\partial Y}\frac{\partial T}{\partial X}+\frac{\partial\Psi}{\partial X}\frac{\partial T}{\partial Y}=\frac{1}{Pr}\left[\frac{1}{Ar^2}\frac{\partial^2 T}{\partial X^2}+\frac{\partial^2 T}{\partial Y^2}\right], \tag{7}$$

where

$$-\zeta=\frac{\partial^2\Psi}{\partial X^2}+Ar^2\frac{\partial^2\Psi}{\partial Y^2}. \tag{8}$$

The initial and boundary conditions in the dimensionless form are

$$\begin{aligned}
&\tau=0: && \Psi=0,\ T=0,\ 0\leqslant X\leqslant 1,\ 0\leqslant Y\leqslant 1,\\
&\tau>0: && \Psi=\frac{\partial\Psi}{\partial Y}=0,\ \frac{\partial T}{\partial X}=0,\ \text{at } X=0 \text{ and } 1,\\
& && \Psi=\frac{\partial\Psi}{\partial X}=0,\ T=1,\ \text{on the hot part at } Y=0,\\
& && \Psi=\frac{\partial\Psi}{\partial X}=0,\ T=0,\ \text{on the cold part at } Y=1,\\
& && \Psi=0,\ \frac{\partial T}{\partial Y}=0,\ \text{at } Y=0 \text{ and } 1.
\end{aligned}$$

The non-dimensional parameters that appear in the equations are $Gr=\frac{g\beta(\theta_h-\theta_c)L^3}{\nu^2}$ the Grashof number, $Pr=\frac{\nu}{\alpha}=0.71$ the Prandtl number, g the acceleration due to gravity, ν the kinematic viscosity, α the thermal diffusivity, β coefficient of thermal expansion, T dimensionless temperature, t time, θ temperature and $Ar=\frac{H}{L}$ the aspect ratio. The local Nusselt number is defined by $Nu=\frac{\partial T}{\partial Y}|_{y=0}$ resulting in the average Nusselt number $\overline{Nu}=\int_h Nu\,dX$, where $h=\frac{H}{2}$ is the length of heating location.

3. Method of solution

A finite volume method based on power law scheme is used to solve numerically the non-dimensional governing equations (6)–(8) by Patankar [14]. The region of interest was covered with m vertical and n horizontal uniformly spaced grid lines. The numerical solution was true-transient and fully implicit. At each time step the vorticity and temperature distributions are obtained from Eqs. (6) and (7), respectively. The stream function distribution was obtained from Eq. (8) using successive over relaxation (SOR) and a known vorticity distribution. The above process is repeated in the next time step until steady state is reached. The dimensionless time step which yields convergence is taken to be $\tau=10^{-5}$. An iterative process is employed to find the stream function, vorticity and temperature fields. The process is repeated until the following convergence criterion is satisfied

$$\left|\frac{\phi_{n+1}(i,j)-\phi_n(i,j)}{\phi_{n+1}(i,j)}\right|\leqslant 10^{-5}. \tag{9}$$

The overall Nusselt number is also used to develop an understanding of the grid fineness that is necessary for accurate numerical simulations. The numerical solutions are found for different grid systems from 21×21 to 101×101. After 41×41 grids, no considerable change in the average Nusselt number is observed and hence a 41×41 grid is used in this study.

4. Results and discussion

Numerical study is conducted for different heating locations, Grashof numbers and aspect ratios. The flow pattern and isotherms for different heating locations, $Ar=2$ and $Gr=10^5$ are displayed in Figs. 2 and 3a–i. The flow is unicellular with clockwise rotation. There exist two secondary

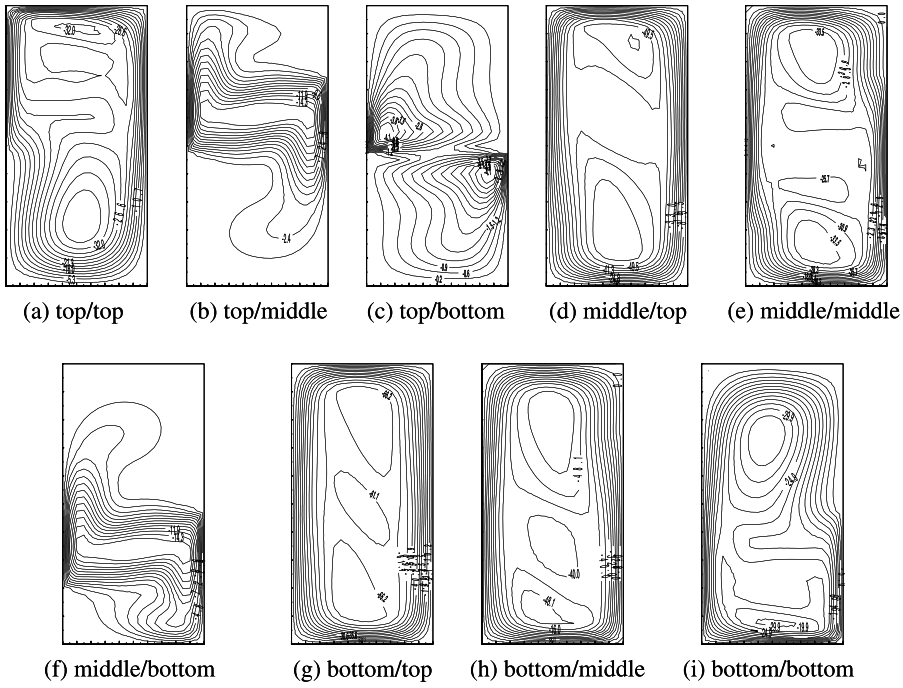

Fig. 2. Streamlines for all heating locations, $Ar = 2$ and $Gr = 10^5$.

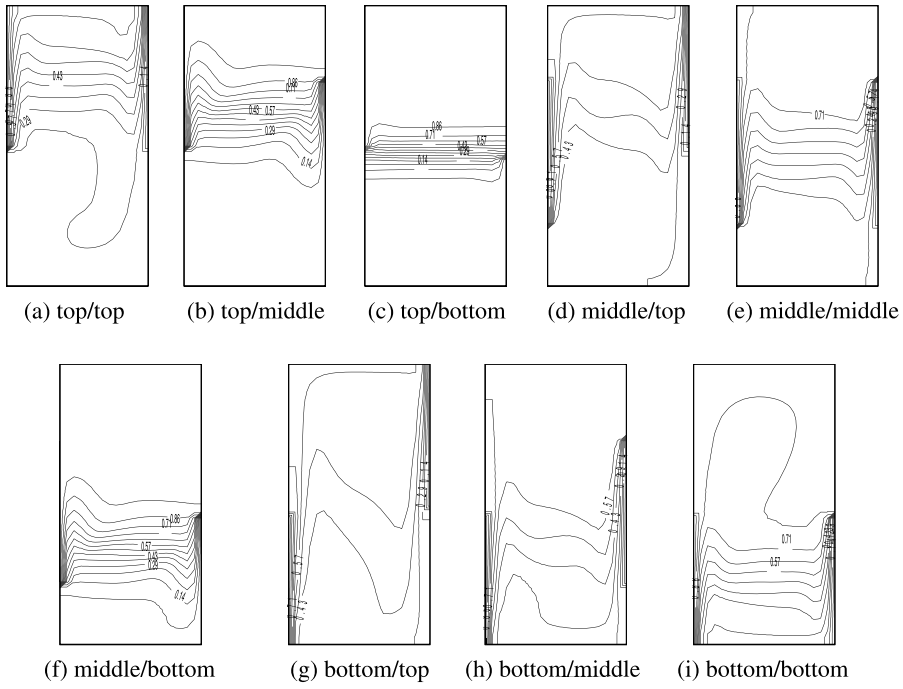

Fig. 3. Isotherms for all heating locations, $Ar = 2$ and $Gr = 10^5$.

cells within the primary cell since both the locations are at the top of the side walls of the cavity, Fig. 2a. The mirror image of the top–top active locations exists for bottom–bottom thermally active locations, as seen in Fig. 2a and i. When the heating location is either top–middle or middle–bottom, the flow is activated around the active zones while the remaining portion of the cavity remains stagnant. It is observed in Fig. 2c that a peculiar phenomenon occurs for the top–bottom thermally active location. The flow is in two cells and centers of the cells are located near the thermally active parts of the side walls. When compared to other positions the heat transfer rate is much less in this

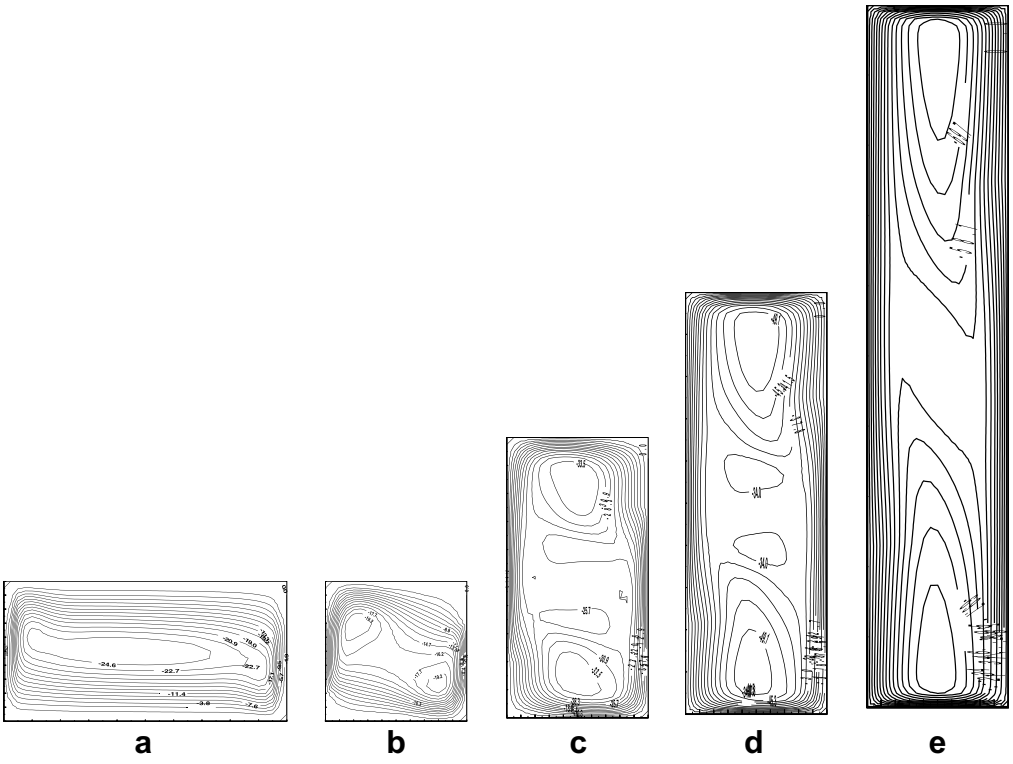

Fig. 4. Streamlines for middle–middle heating location, aspect ratios 0.5, 1, 2, 3 and 5 and $Gr = 10^5$.

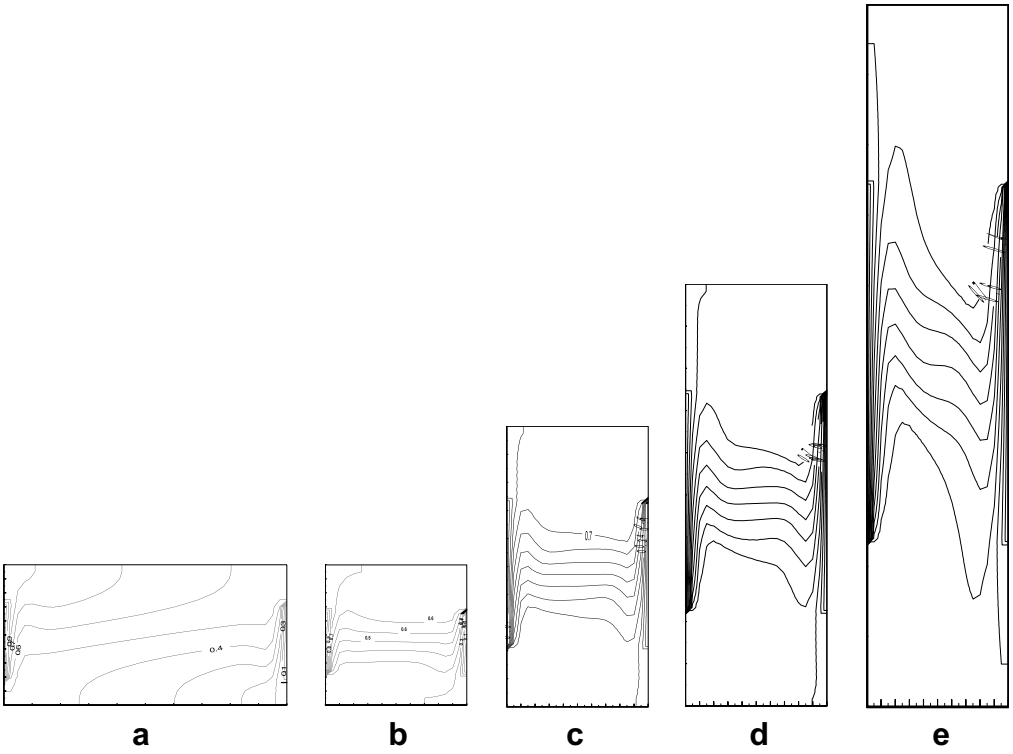

Fig. 5. Isotherms for middle–middle heating location, aspect ratios 0.5, 1, 2, 3 and 5 and $Gr = 10^5$.

case. There exist some small eddies within the clockwise rotating eddy, occupying the whole cavity for all the remaining thermally active zones. The heat transfer rate is maximum at the bottom–top active location.

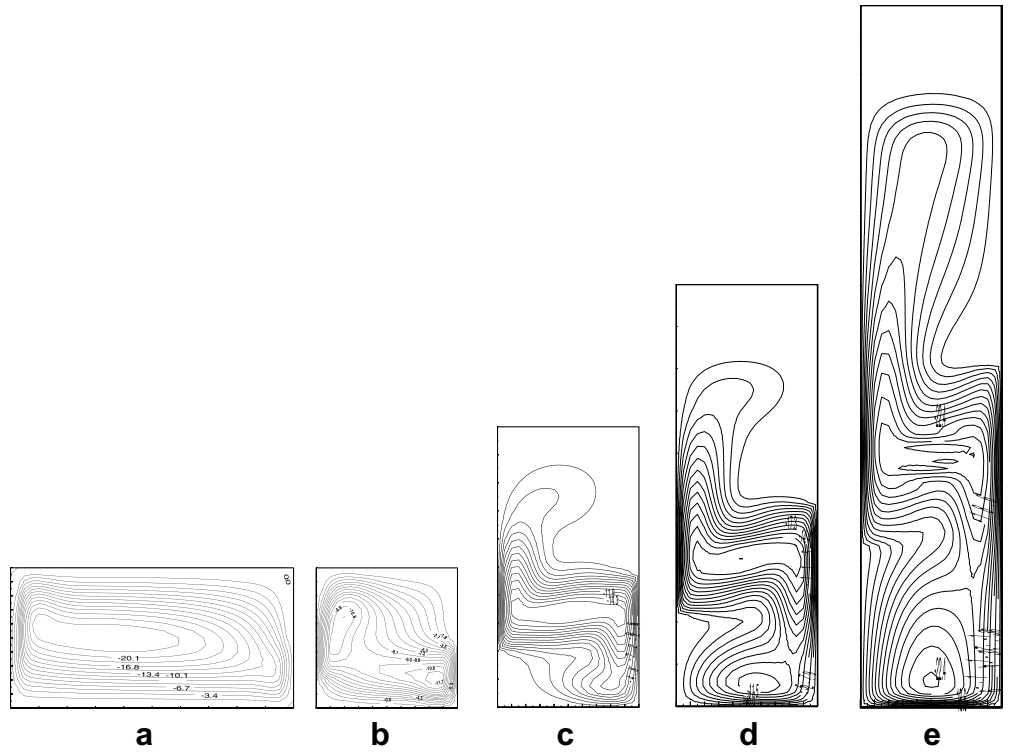

Fig. 6. Streamlines for middle–bottom heating location, aspect ratios 0.5, 1, 2, 3 and 5 and $Gr = 10^5$.

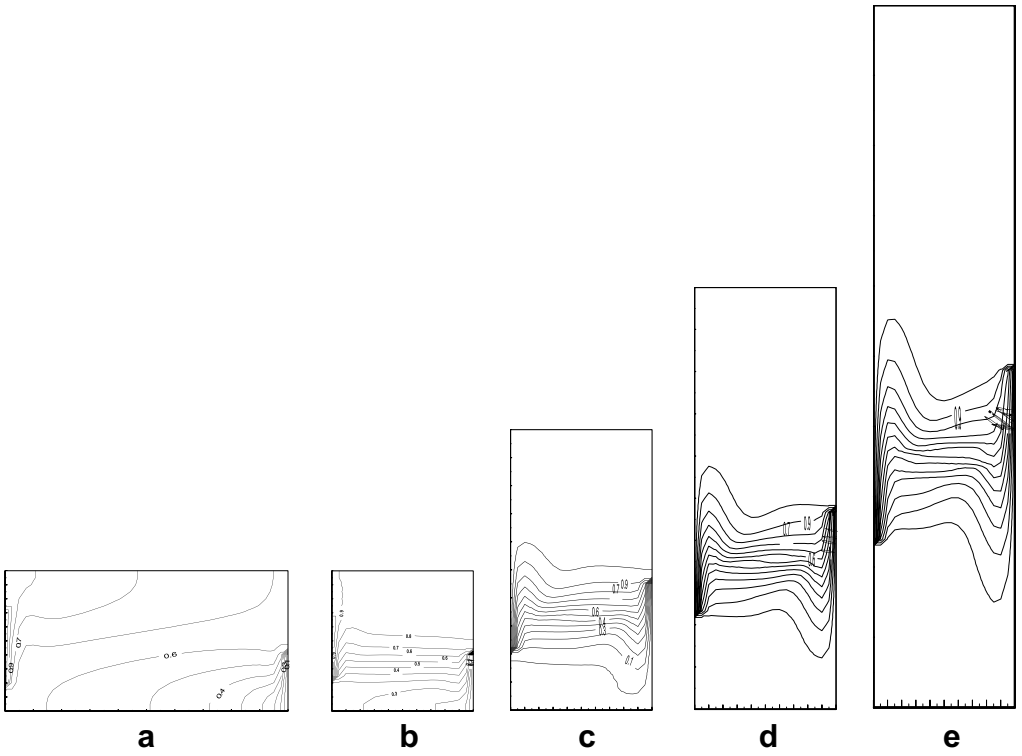

Fig. 7. Isotherms for middle–bottom heating location, aspect ratios 0.5, 1, 2, 3 and 5 and $Gr = 10^5$.

Fig. 3a depicts the convection mode of isotherms mostly at the top region where the active walls are located. When the cold active wall moves from top to bottom, Fig. 3b shows the modifications that the isotherms are transformed

towards conduction at the central region and convection near the active locations. As the cold wall is moved to the bottom, the isotherms predict almost conduction at the middle of the cavity. In this case, the circulation rate and velocity are very low compared to all the other cases. Fig. 3i and f seems to be the mirror images of Fig. 3a and b, respectively. In the middle–top and bottom–middle active locations there is a boundary layer formed at the active walls and the existence of convection is seen from the isotherms of Fig. 3d and h. In Fig. 3e, the middle–middle active location exhibits convection near the active locations. Strong thermal boundary layers are formed at the active locations as seen in Fig. 3g. The circulation rate and the heat transfer rate are maximum in this case compared to all the other cases.

The flow patterns for the middle–middle thermally active location, different aspect ratios and $Gr = 10^5$ are displayed in Fig. 4a–e. When $Ar = 0.5$, in Fig. 4a, a single cell pattern is observed. For the case of square cavity, there exist two inner cells each at the top left and bottom right corners of the cavity. The remaining two corners are less activated but this type of behaviour does not exist in the case of rectangular cavities. The two inner cells are moved to upper and lower parts of the cavity when $Ar = 2$. This is due to the dominating buoyancy force inside the cavity. Further increasing the aspect ratio, the two inner cells grow in size and strength, while two small recirculating eddies occur in the middle of the cavity. Increasing the aspect ratio to 5 the recirculating zones in the middle of the cavity disappear.

The isotherms for the middle–middle thermally active location, different aspect ratios and $Gr = 10^5$ are presented in Fig. 5a–e. For all the aspect ratios, a thermal boundary layer exists along the active zones. Large veloc-

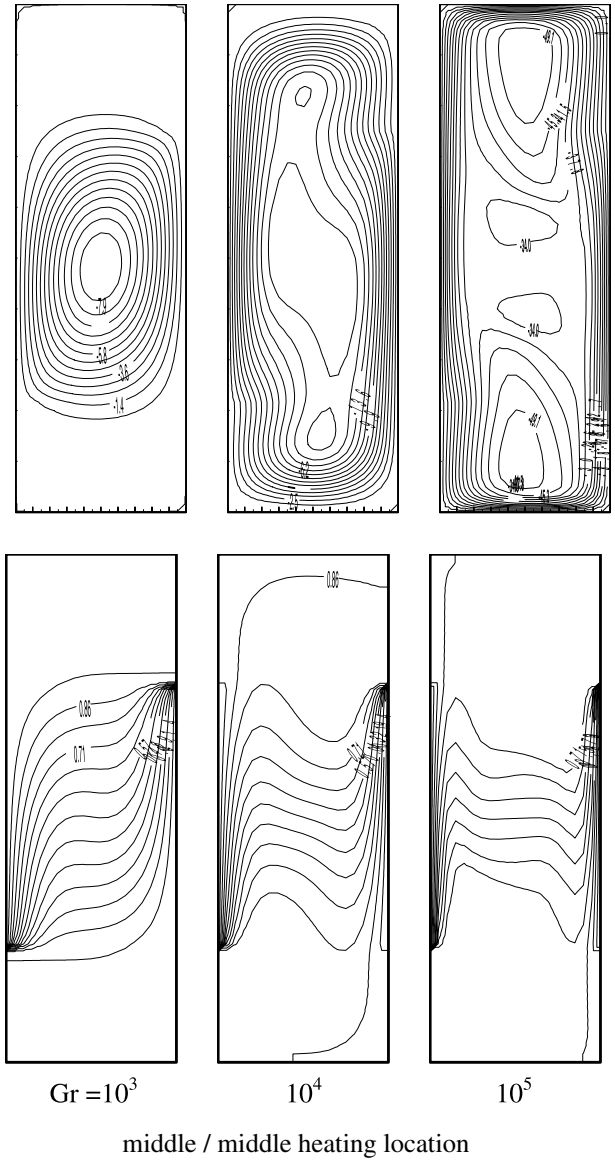

Fig. 8. Streamlines for different Grashof numbers and $Ar = 3$.

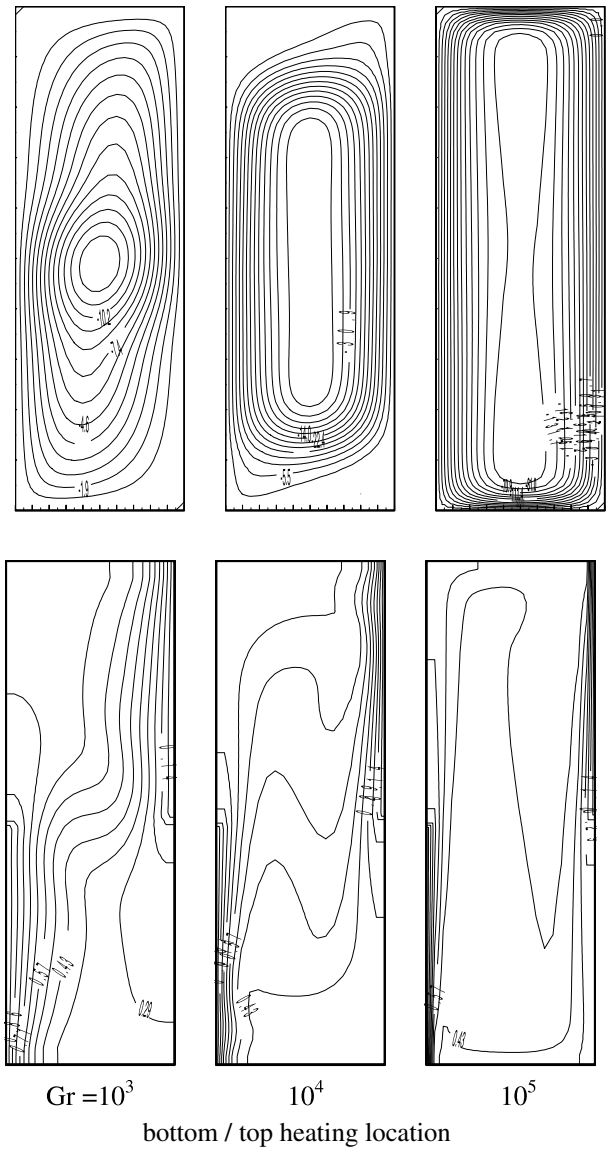

Fig. 9. Isotherms for different Grashof numbers and $Ar = 3$.

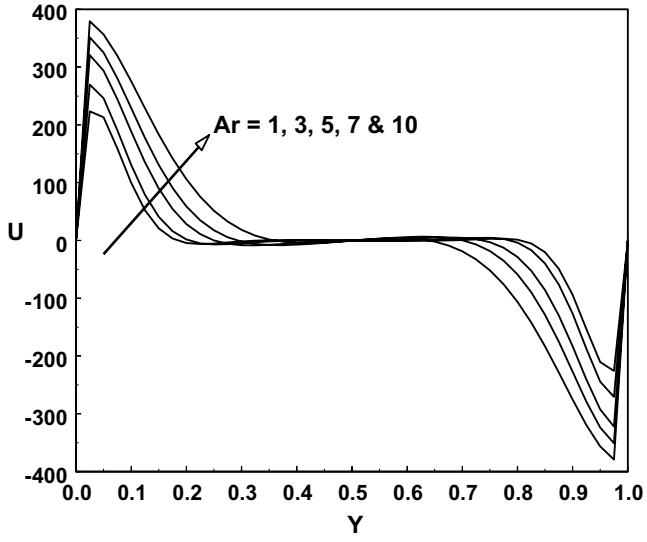

Fig. 10. Mid-height velocity profile for middle–middle heating location and $Gr = 10^5$.

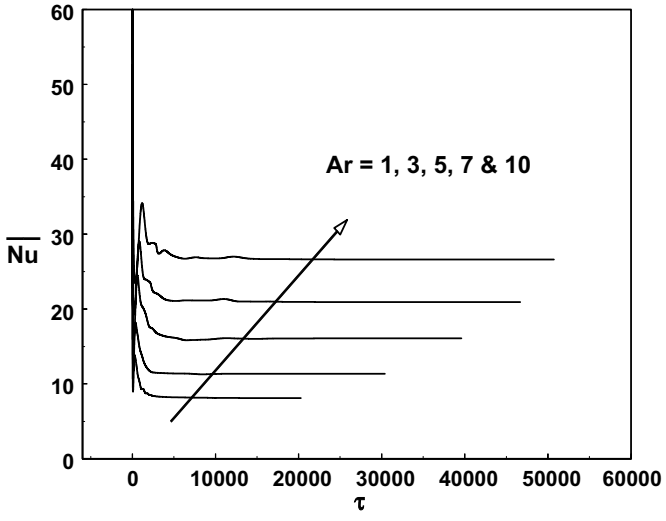

Fig. 11. Time history of average Nusselt number for different, aspect ratios and $Gr = 10^5$.

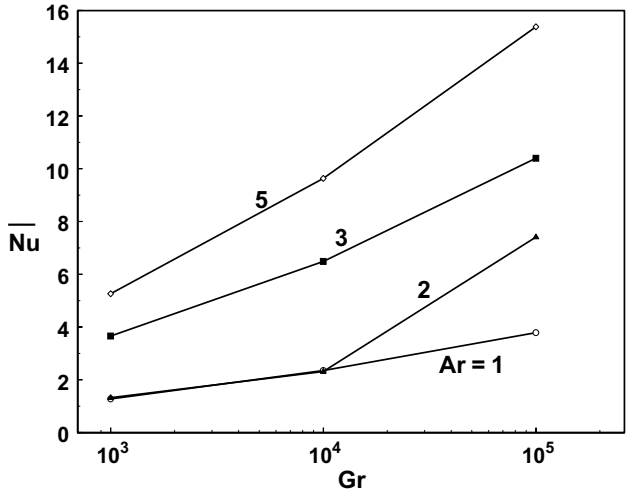

Fig. 12. Average Nusselt number for different aspect ratios.

ity and temperature gradients characterize the region immediately adjacent to the thermally active side wall locations while negligible gradients (normal to the hot/cold wall location) prevail in the rest of the cavity. Such behaviour is indicative of the thermal boundary layer structure.

Fig. 6a–e shows the flow pattern for the middle–bottom thermally active location, different aspect ratios and $Gr = 10^5$. For $Ar = 0.5$, a single cell pattern is observed. In the case of square cavity, the two inner cells exist in the middle left and bottom right active parts of the cavity. On increasing the aspect ratio, the two inner cells disappear and the major cell is skewed upward along the hot wall and downward along the cold wall. Further on increasing the aspect ratio, upper part of the cavity remains stagnant while the lower part of the cavity is more activated. A secondary cell exists within the primary cell in the lower part of the cavity. With increase in the aspect ratio of the cavity, the buoyant convection flow is increasingly strengthened. The isotherms for the middle–bottom thermally active location, for different aspect ratios are displayed in Fig. 7a–e. The same behaviour is observed as in Fig. 5a–e.

Figs. 8 and 9a show the streamlines and isotherms for different Grashof numbers, middle–middle thermally active locations and $Ar = 3$. There exists a clockwise rotating cell in the middle portion of the cavity for $Gr = 10^3$. The fluid in the upper and lower parts of the cavity is stagnant. When $Gr = 10^4$, the circulation rate of the eddy is increased and the unicellular pattern is enlarged and occupies the whole cavity. Further increasing Gr ($=10^5$), there exist four secondary cells inside a large primary cell. Figs. 8 and 9b show the flow pattern and isotherms of the bottom–top thermally active location for different Grashof numbers. For all the values of the Grashof number, there exists a unicellular pattern. The velocity of the fluid particle inside the cavity and also the buoyant convection flow increase by increasing the Grashof number.

Fig. 10 shows the mid-height velocity profile for different aspect ratios and middle–middle thermally active locations. The increase in the vertical velocity of the fluid particles at mid-height of the cavity for increasing aspect ratio near the active locations is shown in Fig. 10. The time history of the average Nusselt number for different aspect ratios and middle–middle active locations are displayed in Fig. 11. Thus the average Nusselt number is increased as the aspect ratio increases. Increasing the aspect ratio

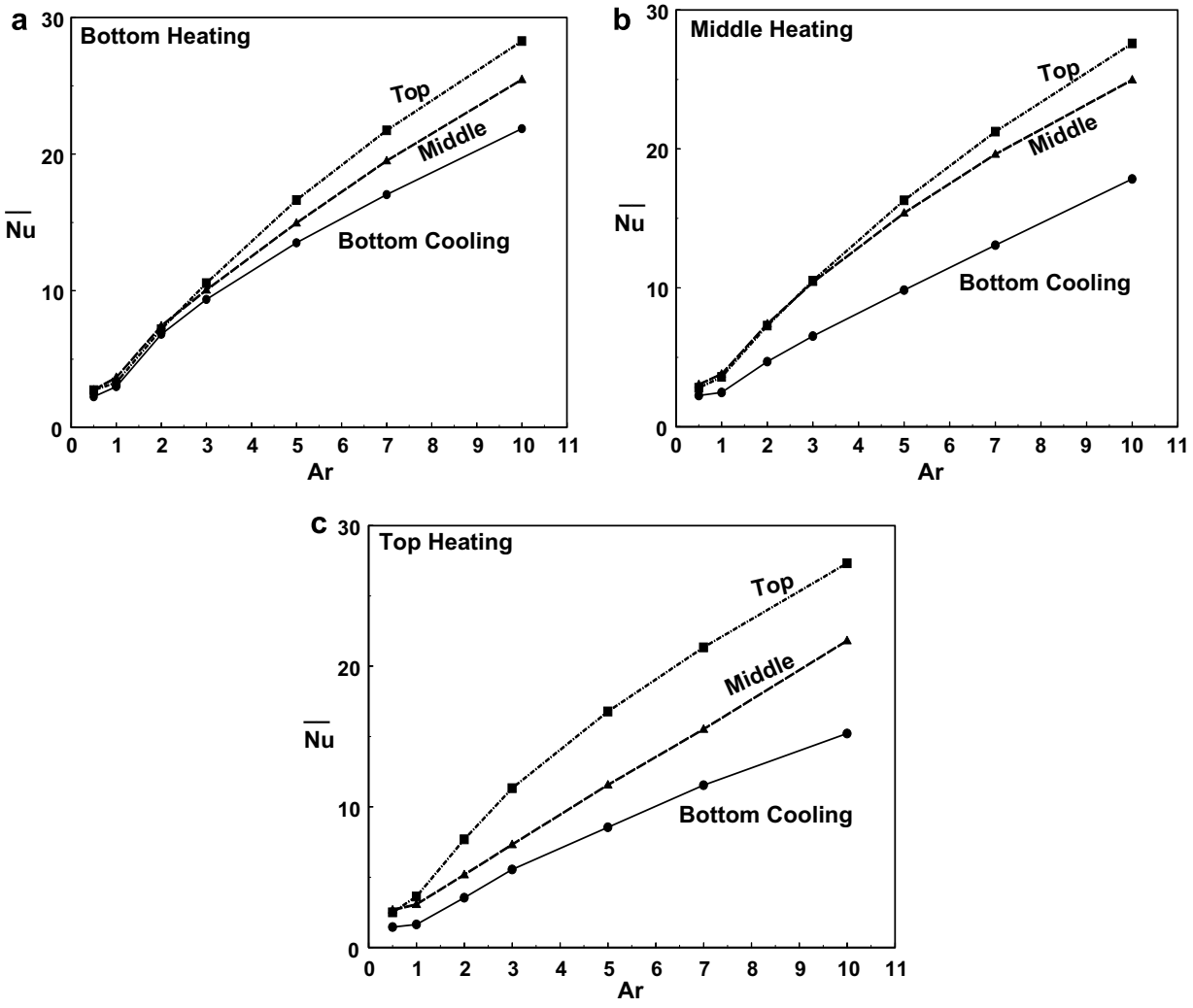

Fig. 13. Average Nusselt number for different heating locations and $Gr = 10^5$.

increases the time to reach the steady state situation of the solution. Average Nusselt number for different aspect ratios, different Grashof numbers and middle–middle thermally active locations is depicted in Fig. 12. The heat transfer rate is increased by increasing both the aspect ratio and the Grashof number.

In order to evaluate how the aspect ratio and different heating locations affect the heat transfer rate, the average Nusselt number is plotted as a function of aspect ratio for different thermally active zones in Figs. 13 and 14. Heat transfer rate is increased on increasing the aspect ratio. There is no considerable variation in the average Nusselt number for $Ar \leqslant 1$ when the heating/cooling locations are changed. But the variation in the average Nusselt number when changing the cooling location is increased by increasing the aspect ratio, Fig. 13a–c. It is observed that from Fig. 14c, there is no remarkable change in the heat transfer rate when the heating location is changed for a fixed cooling location. The heat transfer rate is enhanced when a cooling location is at the top of the enclosure. When changing the heating location from top to bottom the average Nusselt number is increased by increasing the aspect ratio. It is clearly seen from Fig. 14a–c.

5. Conclusions

The heat transfer rate is high for the bottom–top thermally active location while the heat transfer rate is poor in the top–bottom thermally active location. The heat transfer rate is found to increase with increase in the aspect ratio. There is no considerable variation in the heat transfer rate for $Ar \leqslant 1$ when the heating/cooling locations are changed. No remarkable change in the heat transfer rate is observed when the heating location is changed for a fixed cooling location. The heat transfer rate is enhanced when a cooling location is at the top of the enclosure.

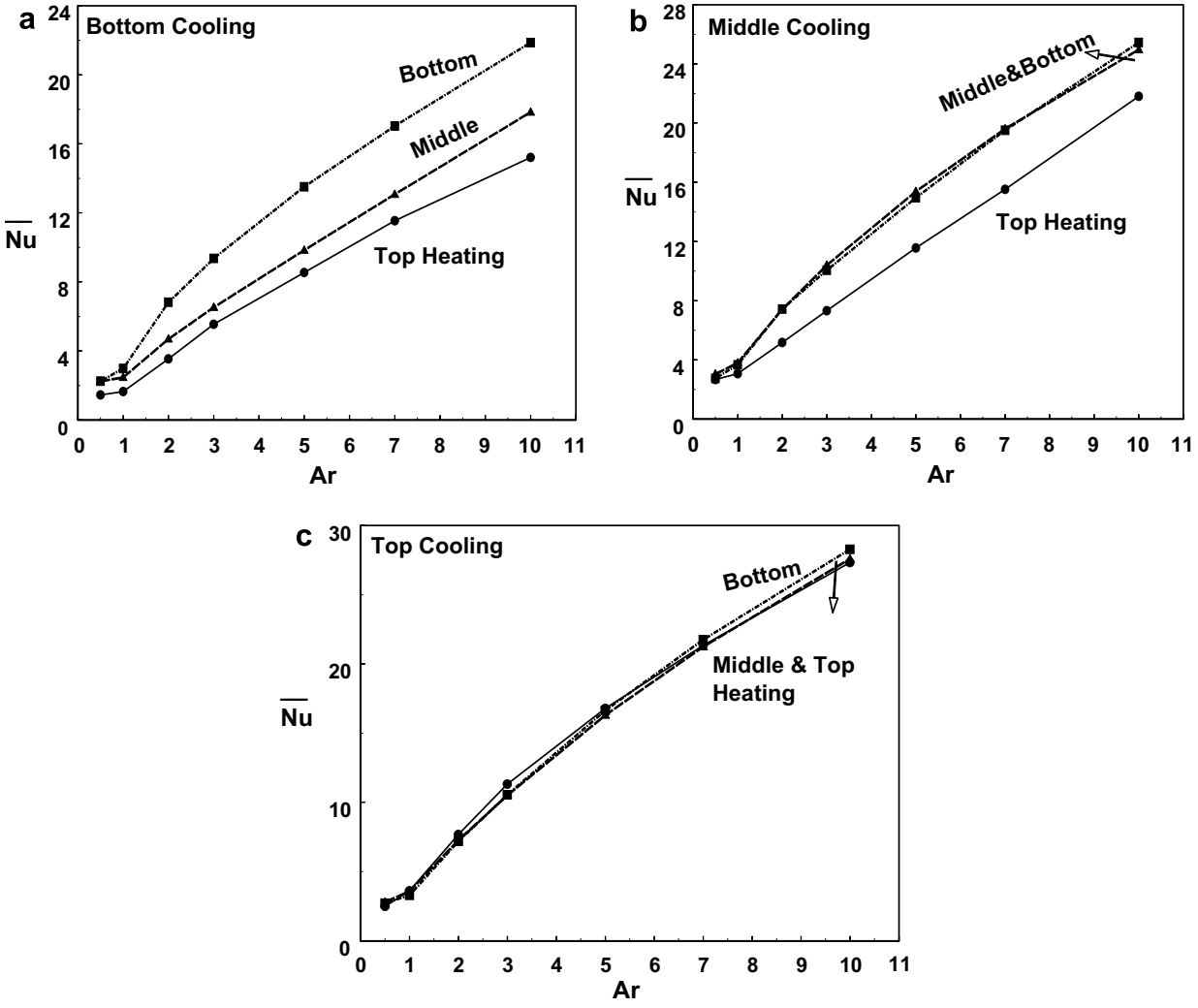

Fig. 14. Average Nusselt number for different cooling locations and $Gr = 10^5$.

References

[1] V. Prasad, F.A. Kulacki, Convective heat transfer in a rectangular porous cavity effect of aspect ratio on flow structure and heat transfer, J. Heat Transfer 106 (1984) 158–165.

[2] S. Paolucci, D.R. Chenoweth, Natural convection in shallow enclosures with differentially heated end walls, J. Heat Transfer 110 (1988) 625–634.

[3] C.J. Ho, J.Y. Chang, A study of natural convection heat transfer in a vertical rectangular enclosure with two-dimensional discrete heating: effect of aspect ratio, Int. J. Heat Mass Transfer 37 (6) (1994) 917–925.

[4] R.L. Frederick, On the aspect ratio for which the heat transfer in differentially heated cavities is maximum, Int. Comm. Heat Mass Transfer 26 (4) (1999) 549–558.

[5] W. Tong, Aspect ratio effect on natural convection in water near its density maximum temperature, Int. J. Heat Fluid Flow 20 (6) (1999) 624–633.

[6] S. Wakitani, Numerical study of three-dimensional oscillatory natural convection at low Prandtl number in rectangular enclosures, J. Heat Transfer 123 (2001) 77–83.

[7] P.K. Das, S. Mahmud, S.H. Tasnim, A.K.M.S. Islam, Effect of surface waviness and aspect ratio on heat transfer inside a wavy enclosure, Int. J. Numer. Meth. Heat Fluid Flow 13 (8) (2003) 1097–1122.

[8] S. Torii, Effect of aspect ratio of unsteady thermal–fluid transport phenomena in cavities under reduced gravity, Int. J. Comput. Eng. Sci. 4 (1) (2003) 85–97.

[9] A. Valencia, R.L. Frederick, Heat transfer in square cavities with partially active vertical walls, Int. J. Heat Mass Transfer 32 (1989) 1567–1574.

[10] M.M. El-Refaee, M.M. Elsayed, N.M. Al-Najem, A.A. Noor, Natural convection in partially cooled tilted cavities, Int. J. Numer. Meth. Fluids 28 (1998) 477–499.

[11] Q.-H. Deng, G.-F. Tang, Y. Li, A combined temperature scale for analyzing natural convection in rectangular enclosures with discrete wall heat sources, Int. J. Heat Mass Transfer 45 (2002) 3437–3446.

[12] N. Nithyadevi, P. Kandaswamy, S. Sivasankaran, Natural convection in a square cavity with partially active vertical walls; time periodic boundary condition, Math. Probl. Eng. 2006 (2006) 1–16.

[13] P. Kandaswamy, S. Sivasankaran, N. Nithyadevi, Buoyancy-driven convection of water near its density maximum with partially active vertical walls, Int. J. Heat Mass Transfer 50 (2007) 942–948.

[14] S.V. Patankar, Numerical Heat Transfer and Fluid Flow, Hemisphere McGraw-Hill, Washington, DC, 1980.